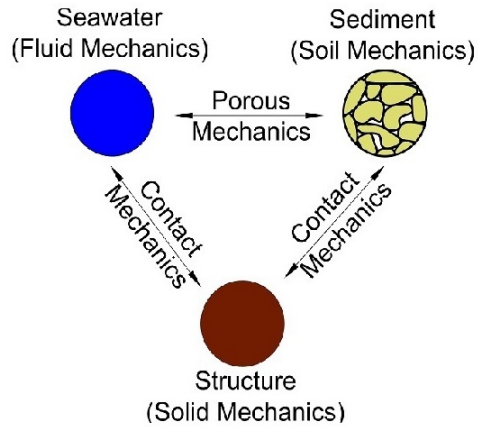
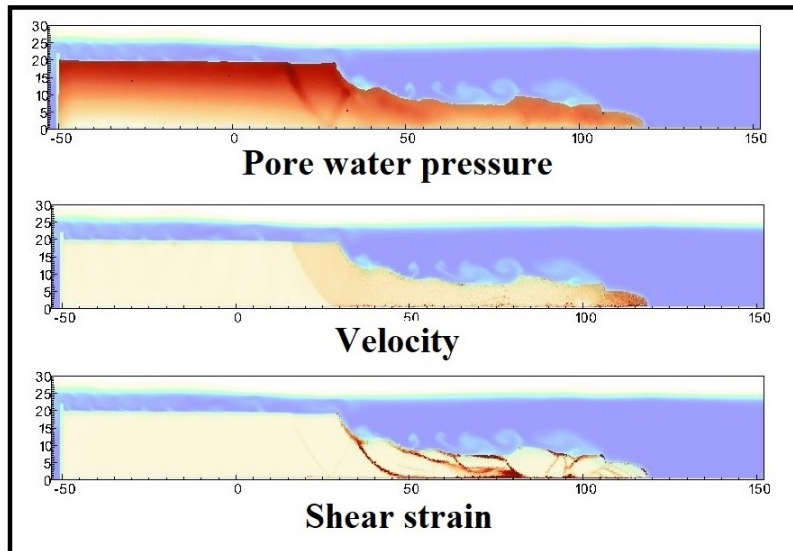


Graphical Abstract

MPMICE: A Lagrangian-Eulerian framework for non-isothermal coupling of deformable porous media and fluid flow



**MPMICE capture complex
soil-fluid-structure interaction**



Application to earthquake-induced submarine landslide

Highlights

MPMICE: A Lagrangian-Eulerian framework for non-isothermal coupling of deformable porous media and fluid flow

- MPMICE is introduced for multiphase flow in porous media.
- Material Point method allows to model large deformation of non-isothermal porous media.
- ICE (compressible multi-material CFD formulation) allows to stabilize pore water pressure and turbulent flow.
- MPMICE is validated and apply to simulate the earthquake-induced submarine landslide.

MPMICE: A Lagrangian-Eulerian framework for non-isothermal coupling of deformable porous media and fluid flow

Abstract

Since offshore structures are expanding significantly, it is critical to estimate potential submarine landslides so that offshore structures can withstand landslides. The complex interaction between saturated sediment, seawater, and offshore structures makes it challenging to simulate submarine landslides. In this paper, a soil-fluid-structure interaction model is presented that combines soil mechanics (saturated sediments), fluid mechanics (seawater), and solid mechanics (structures). The formulation involves coupling the Material Point Method, which models large deformation of porous media, with the Implicit Continuous-fluid Eulerian, which models complex fluid flow. We validate the model and simulate the whole process of earthquake-induced submarine landslides.

Keywords:

Material Point Method, MPMICE, submarine landslide.

Contents

Nomenclature	4
Introduction	6
Theory and formulation	7
Assumptions	7
Governing equations	7
Equation of state for fluid phases	9
Constitutive soil model	10
Momentum and Energy exchange model	11
Solving momentum exchange with an implicit solve	12
Turbulent model	12
Numerical implementation	13
Interpolation from Solid Particle to Grid	13
Compute equation of state for fluid phase	14
Compute faced-centered velocity	14
Compute advanced fluid pressure (implicit scheme)	15
Compute viscous shear stress term of the fluid phase	15
Compute nodal internal temperature of the solid phase	16
Compute and integrate acceleration of the solid phase	16
Compute Lagrangian value (mass, momentum and energy)	16
Compute Lagrangian specific volume of the fluid phase	17
Compute advection term and advance in time	18
Interpolate from cell to node of the solid phase	18
Update the particle variables	19
Numerical examples	19
Fluid Flow through isothermal porous media	19
Isothermal consolidation	20
Thermal induced cavity flow	21
Underwater debris flow	22
Earthquake-induced submarine landslides	25
Conclusions	26
Acknowledgements	26

Appendix	26
Evolution of porosity	28
Evolution of specific volume	29
Momentum conservation	30
Energy conservation	31
Advanced Fluid Pressure	32
Momentum exchange with an implicit solve	32

Nomenclature

General variables

<u>Variable</u>	<u>Dimensions</u>	<u>Description</u>
V	$[L^3]$	Representative volume
n		Porosity
σ	$[M/L^2]$	Total stress tensor
Δt	$[t]$	Time increment
\mathbf{b}	$[L/t]$	Gravity acceleration
c_v	$[L^2/t^2]$	Constant volume specific heat
f_d	$[ML//t^2]$	Drag forces in momentum exchange term
f^{int}	$[ML//t^2]$	Internal forces
f^{ext}	$[ML//t^2]$	External forces
q_{fs}	$[ML//t^2]$	Heat exchange term
S		Shape function
∇S		Gradient of shape function

Solid phase

<u>Variable</u>	<u>Dimensions</u>	<u>Description</u>
m_s	$[M]$	Solid mass
ρ_s	$[M/L^3]$	Solid density
ϕ_s	$-]$	Solid volume fraction
$\bar{\rho}_s$	$[M/L^3]$	Average Solid density
\mathbf{x}_s	$[L]$	Solid Position vector
\mathbf{U}_s	$[L/t]$	Solid Velocity vector
\mathbf{U}'_s	$[L/t]$	Solid Velocity gradient vector
\mathbf{a}_s	$[L/t^2]$	Solid Acceleration vector
σ'	$[M/L^2]$	Effective Stress tensor
e_s	$[L^2/t^2]$	Solid Internal energy
T_s	$[T]$	Solid Temperature
\mathbf{F}_s		Solid Deformation gradient
V_s	$[L^3]$	Volume

Fluid phase		
<u>Variable</u>	<u>Dimensions</u>	<u>Description</u>
m_f	[M]	Fluid mass
ρ_f	[M/L ³]	Fluid density
ϕ_f	[—]	Fluid volume fraction
$\bar{\rho}_f$	[M/L ³]	Average Fluid density
\mathbf{U}_f	[L/t]	Fluid Velocity vector
$\boldsymbol{\sigma}_f$	[M/L ²]	Fluid stress tensor
Δp_f	[M/L ²]	Fluid isotropic pressure
$\boldsymbol{\tau}_f$	[M/L ²]	Fluid shear stress tensor
p_f	[M/L ²]	Isotropic pressure
e_f	[L ² /t ²]	Fluid Internal energy ($c_v T_f$) of the material per unit mass
T_f	[T]	Fluid Temperature
v_f	[L ³ /M]	Fluid Specific volume $\frac{1}{\rho_f}$
α_f	[1/T]	Thermal expansion
μ	[M/L ² T]	Fluid viscosity
Superscript		
<u>Variable</u>	<u>Dimensions</u>	<u>Description</u>
n		Current time step
L		Lagrangian values
$n + 1$		Next time step
Subscript		
c		Cell-centered quantity
p		Particle quantity
i		Node quantity
FC		Face-centered quantity
L, R		Left and Right cell faces

Table 1: Nomenclature

Introduction

Submarine landslides can pose significant threats to the offshore infrastructures and the coastal communities. Submarine landslides have three stages: triggering, failure, and post-failure. Erosion or earthquakes can trigger slope failures in the first stage. Following the failure, sediments move quickly after the post-failure stage. As a submarine landslide is triggered, sediment behaves like solid (soil) materials and changes to fluid-like behavior after failure. This phase transition makes it challenge to simulate the submarine landslides.

Due to this phase transition, submarine landslide can be modeled by either the Computational Fluid Dynamics (CFD) or the particle-based methods. For simulating submarine slides, CFD methods solve governing equations in a full-Eulerian framework for single-phase flows [1, 2] and for multi-phase flows [3, 4] with interface capturing techniques. While CFD can handle complex flows (such as turbulent flows), it cannot account for the triggering mechanism of submarine landslides because it is not straightforward to consider 'soil constitutive laws' of sediment materials in the Eulerian framework. In contrast, particle-based methods can overcome this problem by using the Lagrangian framework. These methods have been extensively used to simulate landslides, like Material Point Method (MPM) [5], Smooth Particle Hydro Dynamics [6], Particle Finite Element Method [7], or Coupled Eulerian Lagrangian Method [8]. For simplicity, these simulations adopt total stress analysis which neglects the pore pressure development which is the key factor triggering slope failures.

Recent developments in particle-based methods model the coupling of fluid flow in porous media by sets of Lagrangian particles. For the MPM family, it is the double-point MPM ([9, 10, 11]) where fluid particles and solid particles are overlapped in a single computational grid. Even if fluid flows are considered, particle-based methods have numerical instability in modeling the fluid flow, which requires additional numerical treatments such as the B-bar method [9], null-space filter [12], or least square approximation [13, 14]. Indeed, CFD is a more optimal option for complex fluid flows especially dealing with large distortions of continuum fluid media. Therefore, it could be ideal to combine the CFD with particle-based methods. More than 50 particle-based methods have been developed to solve large deformations

of solids over the last two decades [15], but the MPM appears to be the best candidate for coupling with the CFD. Because MPM incorporates a stationary mesh during computation, just like CFD. As such, both MPM and CFD can be coupled naturally in a unified computational mesh.

The work presented here describes a numerical approach for simulation of soil-fluid-structure interaction involving large deformation using the coupling the ICE (CFD with the MPM). In brief

Theory and formulation

This section lay out the theoretical framework for the MPMICE model. We use the common notation of the continuum mechanics with vector and tensor denoted simply by using bold font and scalar denoted by using normal font. The notation are shown in Table 1.

Assumptions

The following assumptions are made for the MPMICE model.

1. Solid phase (MPM) is described in a Lagrangian formulation while fluid phase (ICE) are described in an Eulerian formulation in the framework of continuum mechanics and mixture theory.
2. Solid grains are incompressible while the fluid phase is compressible.
3. There is no mass exchange between solid and fluid phases.
4. Terzaghi's effective stress is valid.

Governing equations

A representative element volume Ω is decomposed by two domains: solid domains Ω_s and fluid domains Ω_f . Then, all domains are homogenized into two overlapping continua. Considering the volume fraction of solid $\phi_s = \Omega_s/\Omega$ and fluid $\phi_f = \Omega_f/\Omega$ with the true (or Eulerian) porosity $n = \sum \phi_f$ of the representative element volume, the average density of solid and fluid phase are defined as:

$$\bar{\rho}_s = \phi_s \rho_s, \quad \bar{\rho}_f = \phi_f \rho_f \quad (1)$$

The mass of solid and fluid phase are:

$$m_s = \int_{\Omega} \rho_s dV = \bar{\rho}_s V, \quad m_f = \int_{\Omega} \rho_f dV = \bar{\rho}_f V \quad (2)$$

Reviewing the Terzaghi's effective stress concept for the saturated porous media, the total stress $\boldsymbol{\sigma}$ is calculated by:

$$\boldsymbol{\sigma} = \boldsymbol{\sigma}' - p_f \mathbf{I} \quad (3)$$

The balance equations are derived based on the mixture theory. The average thermodynamic state of the fluid phase is given by the vector $[m_f, \mathbf{U}_f, e_f, T_f, v_f]$ which are mass, velocity, internal energy, temperature, specific volume. The average state of the solid phase is given by the vector $[m_s, \mathbf{U}_s, e_s, T_s, \boldsymbol{\sigma}']$ which are mass, velocity, internal energy, temperature, effective stress. Here, we summarize the final form of the equations while the derivation is presented in detail in the Appendix.

Mass Conservation

The mass balance equations for both fluid and solid phase are

$$\frac{1}{V} \frac{D_f m_f}{Dt} = 0, \frac{1}{V} \frac{D_s m_s}{Dt} = 0 \quad (4)$$

Solving the solid mass and the fluid mass balance equation leading to the rate of the specific volume as

$$\bar{\rho}_f \frac{D_f v_f}{Dt} = \nabla \cdot ((1-n)\mathbf{U}_s + n\mathbf{U}_f) \quad (5)$$

Momentum Conservation

The momentum balance equation for the fluid phase is

$$\frac{1}{V} \frac{D_f(m_f \mathbf{U}_f)}{Dt} = -n \nabla P_{eq} + \nabla \cdot \boldsymbol{\tau}_f + \bar{\rho}_f \mathbf{b} + \mathbf{f}_d \quad (6)$$

The momentum balance equation for the solid phase is

$$\frac{1}{V} \frac{D_s(m_s \mathbf{U}_s)}{Dt} = \nabla \cdot (\boldsymbol{\sigma}') - (1-n) \nabla p_f + \bar{\rho}_s \mathbf{b} - \mathbf{f}_d \quad (7)$$

Energy Conservation

The internal energy balance equation for the fluid phase is

$$\frac{1}{V} \frac{D_f(m_f e_f)}{Dt} = -\bar{\rho}_f P_{eq} \frac{D_f v_f}{Dt} + \boldsymbol{\tau}_f : \nabla \mathbf{U}_f + \nabla \cdot \mathbf{q}_f + q_d \quad (8)$$

The internal energy balance equation for the solid phase is

$$\frac{1}{V} \frac{D_s(m_s e_s)}{Dt} = \boldsymbol{\sigma}' : \nabla \mathbf{U}_s + \nabla \cdot \mathbf{q}_s - q_d \quad (9)$$

Furthermore, to close the systems of the equations, it requires the additional models: (1) An equation of state to establish relations between thermodynamics variables $[P_{eq}, \rho_f, T_f]$. (2) A constitutive equation to describe the stress - strain behaviour of solid phase. (3) Exchange momentum model. (4) Energy exchange model. (5) Optional turbulent model to compute the viscous shear stress τ_f .

Equation of state for fluid phases

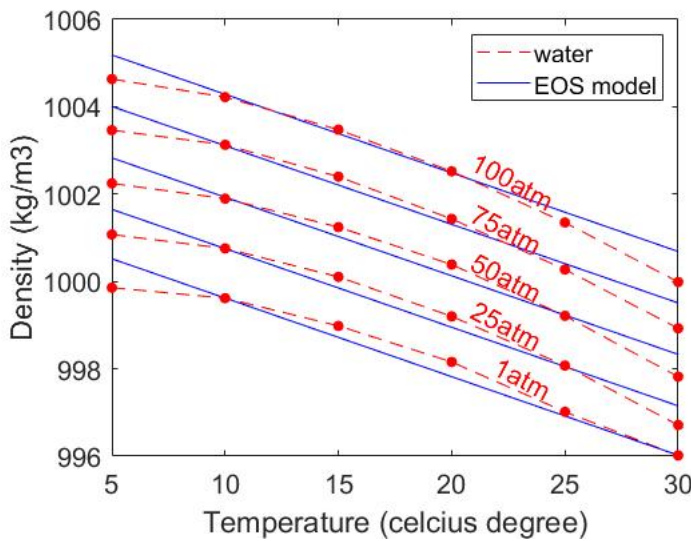


Figure 1: Equation of state of water

The equation of state establishes relations between thermodynamics variables $[P_{eq}, \rho_f, T_f]$. Here, P_{eq} is "equilibrium" pressure which is defined as pressure enables mass of fluid material to fills in an entire porosity volume with no ongoing compression or expansion with given true density ρ_f and temperature T_f . The choice of the equation of state depends on the types of the fluid materials. For example, for the air, it is possible to assume the

equation of state for the perfect gas which obeys:

$$P_{eq} = \rho_f R T_f \quad (10)$$

where R is the gas constant. For the water, a simple linear equation of state is in the following form:

$$P_{eq} = P_{ref} + K_f (\rho_f - \rho_{ref} - \alpha_f (T_f - T_{ref})) \quad (11)$$

where reference pressure $P_{ref} = 1 \text{ atm} = 101325 \text{ Pa}$, reference temperature $T_{ref} = 10^\circ\text{C}$, reference density $\rho_{ref} = 999.8 \text{ kg/m}^3$, the bulk modulus of water $K_f = 2 \text{ GPa}$, and the water thermal expansion $\alpha_f = 0.18 \text{ kg/m}^3 \text{ per Celsius degree}$. Equation (11) matches well with the state of the water (see Figure 1).

Constitutive soil model

As a result of the explicit MPM formulation, we can derive the constitutive law in the updated Lagrangian framework of "small strain - large deformation". Therefore, the rotation of the particles (representative element volume) is manipulated by rotating the Cauchy stress tensor. First, the deformation gradient is decomposed into the polar rotation tensor \mathbf{R}_s^{n+1} and sketch tensor \mathbf{V}_s^{n+1} as

$$\mathbf{F}_s^{n+1} = \mathbf{V}_s^{n+1} \mathbf{R}_s^{n+1} \quad (12)$$

Then, before calling the constitutive model, the stress and strain rate tensor are rotated to the reference configuration as

$$\boldsymbol{\sigma}'^{n*} = (\mathbf{R}_s^{n+1})^T \boldsymbol{\sigma}'^{n*} \mathbf{R}_s^{n+1} \quad (13)$$

$$\delta\boldsymbol{\epsilon}^{n*} = (\mathbf{R}_s^{n+1})^T \delta\boldsymbol{\epsilon}_s^{n*} \mathbf{R}_s^{n+1} \quad (14)$$

Using the constitutive model with the input tensors $\boldsymbol{\sigma}'^{n*}, \delta\boldsymbol{\epsilon}^{n*}$ to compute the Cauchy stress tensor at the advanced time step $\boldsymbol{\sigma}'^{n+1*}$ then rotating it back to current configuration

$$\boldsymbol{\sigma}'^{n+1} = \mathbf{R}_s^{n+1} \boldsymbol{\sigma}'^{n+1*} (\mathbf{R}_s^{n+1})^T \quad (15)$$

In this paper, we adopt the hyper-elastic Neo Hookean model for the structure materials and additionally Mohr-Coulomb failure criteria for the soil (porous

media) materials. The Cauchy stress of the Neo Hookean model can be written as:

$$\boldsymbol{\sigma}' = \frac{\lambda \ln(J)}{J} + \frac{\mu}{J} (\mathbf{F} \mathbf{F}^T - \mathbf{J}) \quad (16)$$

where λ and μ are bulk and shear modulus ad J is the determinant of the deformation gradient \mathbf{F} . And the yield function f and flow potentials g of the Mohr-Coulomb can be written as:

$$\begin{aligned} f &= \sigma'_1 - \sigma'_3 - 2c' \cos(\phi') - (\sigma'_1 + \sigma'_3) \sin(\phi') \\ g &= \sigma'_1 - \sigma'_3 - 2c' \cos(\psi') - (\sigma'_1 + \sigma'_3) \sin(\psi') \end{aligned} \quad (17)$$

where the c' , ϕ' and ψ' are cohesion and friction angle and dilation angle. σ'_1 and σ'_3 are maximum and minimum principal stress.

Momentum and Energy exchange model

Currently, the energy exchange coefficient is assumed to be constant for the sake of simplicity. For the momentum exchange, we assume that the drag force \mathbf{f}_d depends on the average grain size of the grains D_p , the porosity n , the fluid viscosity μ_f , and is propotional to the relative velocities of soil grains and fluid $(\mathbf{U}_s - \mathbf{U}_f)$. Therefore, The drag force following the Darcy law is given by:

$$\mathbf{f}_d = \frac{18\phi_s(1-\phi_s)\mu_f}{D_p^2} F(\phi_s, Re) (\mathbf{U}_s - \mathbf{U}_f) \quad (18)$$

where Reynolds number Re are computed as:

$$Re = \frac{n\rho_f D_p}{\mu_f} \|\mathbf{U}_s - \mathbf{U}_f\| \quad (19)$$

Based on recent investigation of CFD simulations of fluid flow around mono- and bi-disperse packing of spheres for $0.1 < \phi_s < 0.6$ and $Re < 1000$ [16]. The function $F(\phi_s, Re)$ can be calculated as:

$$F(\phi_s, Re) = F(\phi_s, 0) + \frac{0.413Re}{24(1-\phi_s)^2} \left(\frac{(1-\phi_s)^{-1} + 3\phi_s(1-\phi_s) + 8.4Re^{-0.343}}{1 + 10^{3\phi_s} Re^{-(1+4\phi_s)/2}} \right) \quad (20)$$

where the low Reynold coefficient $F(\phi_s, Re \rightarrow 0)$ is:

$$F(\phi_s, 0) = \frac{10\phi_s}{(1-\phi_s)^2} + (1-\phi_s)^2(1 + 1.5\sqrt{\phi_s}) \quad (21)$$

In the paper, we convert the equation 18 to Kozeny-Carman formula by assuming $F(\phi_s, Re) = 10\phi_s/(1 - \phi_s)^2$, then, the hydraulic conductivity will be expressed as $K = d^2(1 - \phi_s)^3/180\mu\phi_s^2$.

Solving momentum exchange with an implicit solve

In this study, we apply the Darcy's law to compute the momentum exchange term. The derivation of the implicit integration for the momentum exchange is presented in the section 'Momentum exchange with an implicit solve'. The linear equations has the form:

$$\begin{vmatrix} (1 + \beta_{12}) & -\beta_{12} \\ -\beta_{21} & (1 + \beta_{21}) \end{vmatrix} \begin{vmatrix} \Delta \mathbf{U}_f \\ \Delta \mathbf{U}_s \end{vmatrix} = \begin{vmatrix} \beta_{12}(\mathbf{U}_s^* - \mathbf{U}_f^*) \\ \beta_{21}(\mathbf{U}_f^* - \mathbf{U}_s^*) \end{vmatrix}$$

where the intermediate velocity can be calculated by

$$\begin{aligned} \mathbf{U}_f^* &= \mathbf{U}_f^n + \Delta t \left(-\frac{\nabla P_f^{n+1}}{\rho_f^n} + \frac{\nabla \cdot \boldsymbol{\tau}_f^n}{\bar{\rho}_f^n} + \mathbf{b} \right) \\ \mathbf{U}_s^* &= \mathbf{U}_s^n + \Delta t \left(\frac{\nabla \cdot \boldsymbol{\sigma}'^n}{\bar{\rho}_s^n} - \frac{\nabla P_f^{n+1}}{\rho_s} + \mathbf{b} \right) \end{aligned} \quad (22)$$

Also, the momentum exchange coefficient can be computed at every time step as $\beta_{12} = K/\bar{\rho}_f^n$ and $\beta_{21} = K/\bar{\rho}_s^n$ with Cauchy coefficient $K = 18\phi_s(1 - \phi_s)\mu_f F(\phi_s, Re)/D_p^2$.

Turbulent model

The turbulent effect is modelled using a statistical approach namely large-eddy simulation. In this approach, the micro-scale turbulent influence in the dynamics of the macro-scale motion is computed through simple models like Smagorinsky model. In the Smagorinsky mode, the residual stress tensor is:

$$\tau_{ij} = 2\mu_{eff}(\bar{S}_{ij} - \frac{1}{3}\delta_{ij}\bar{S}_{kk}) + \frac{1}{3}\delta_{ij}\tau_{kk} \quad (23)$$

where the the strain rate tensor is given by

$$\bar{S}_{ij} = \frac{1}{2} \left(\frac{\delta \bar{\mathbf{U}}_i}{\delta x_j} + \frac{\delta \bar{\mathbf{U}}_j}{\delta x_i} \right) \quad (24)$$

and the effective viscosity is sum of molecular viscosity and turbulent viscosity $\mu_{eff} = \mu + \mu_t$ in which the turbulent viscosity μ_t is calculated by

$$\mu_t = (C_s \Delta)^2 \sqrt{2\bar{S}_{ij}\bar{S}_{ij}} \quad (25)$$

where C_s is the Smagorinsky constant and $\Delta = \sqrt[3]{dx dy dz}$ is the grid size that defines the subgrid length scale.

Numerical implementation

The fluid phase is discretized in the grid with the state variables stored at the centroid of the cells $[\rho_{fc}, \mathbf{U}_{fc}, T_{fc}, v_{fc}]$ while the solid phase is discretized in the particles with the state variables $[m_{sp}, \mathbf{U}_{sp}, T_{sp}, \boldsymbol{\sigma}'_{sp}]$. The numerical implementation based on the MPMICE implementation in Uintah from cite MPMICE. The weak forms of the governing equation are solved using the following steps:

Interpolation from Solid Particle to Grid

The nodal values of the solid state (mass, velocity, temperature, volume) are:

$$\begin{aligned} m_{si}^n &= \sum S_{ip} m_{sp} \\ \mathbf{U}_{si}^n &= \frac{\sum S_{ip} (m\mathbf{U})_{sp}^n}{m_{si}^n} \\ T_{si}^n &= \frac{\sum S_{ip} (mT)_{sp}^n}{m_{si}^n} \\ V_{si}^n &= \frac{\sum S_{ip} (mV)_{sp}^n}{m_{si}^n} \\ \boldsymbol{\sigma}_{si}^n &= \frac{\sum S_{ip} (\boldsymbol{\sigma}V)_{sp}^n}{V_{si}^n} \end{aligned} \quad (26)$$

The nodal internal forces is calculated by

$$\mathbf{f}_{si}^{int,n} = - \sum \nabla S_{ip} (\boldsymbol{\sigma}'_{sp})^n V_{sp}^n \quad (27)$$

The nodal external forces $f_{si}^{ext,n}$ and extra momentum from contact forces are computed here. The nodal velocity and nodal temperature are applied boundary conditions.

Then we compute the solid cell variables as:

$$\begin{aligned}
m_{sc}^n &= \sum S_{ci} m_{si} \\
\rho_{sc}^n &= \frac{m_{sc}^n}{V} \\
\mathbf{U}_{sc}^n &= \sum S_{ci} \mathbf{U}_{si}^n \\
T_{sc}^n &= \sum S_{ci} T_{si}^n \\
V_{sc}^n &= \sum S_{ci} V_{si}^n \\
\boldsymbol{\sigma}_{sc}^n &= \sum S_{ci} \boldsymbol{\sigma}_{si}^n
\end{aligned} \tag{28}$$

Compute equation of state for fluid phase

Here the

For the air, it is possible to assume the equation of state for the perfect gas which obeys:

$$P_{eq} = \rho R T \tag{29}$$

where R is the gas constant. For the water, the equation of state (Thomsen Hartka water model) can be used to obtain the relations between the thermodynamic properties of the water.

Compute faced-centered velocity

Following the derivation in the Appendix: Advanced Fluid Pressure, we first compute the fluid face-centered velocity as

$$\mathbf{U}_{f,FC}^* = \frac{(\bar{\rho} \mathbf{U})_{f,FC}^n}{\bar{\rho}_{f,FC}^n} + \Delta t \left(-\frac{\nabla^{FC} P_{eq}}{\bar{\rho}_{f,FC}^n} + \frac{\nabla^{FC} \cdot \boldsymbol{\tau}^n}{\bar{\rho}_{s,FC}} + \mathbf{b} \right) \tag{30}$$

The equation (30) is discretized in three dimension (noted that $\nabla^{FC} \cdot \boldsymbol{\tau} = 0$), for example the discretized equation in the x direction is

$$U_{fx}^* = \frac{(\bar{\rho} U)_{fx,R}^n + (\bar{\rho} U)_{fx,L}^n}{\bar{\rho}_{fx,L}^n + \bar{\rho}_{fx,R}^n} + \Delta t \left(-\frac{2(v_{fx,L}^n v_{fx,R}^n)}{v_{fx,L}^n + v_{fx,R}^n} \frac{P_{eqx,R} - P_{eqx,L}}{\Delta x} + b_x \right) \tag{31}$$

The face-centered solid velocity can be calculated as

$$\mathbf{U}_{s,FC}^* = \frac{(\bar{\rho} \mathbf{U})_{s,FC}^n}{\bar{\rho}_{s,FC}^n} + \Delta t \left(\frac{\nabla^{FC} \cdot \boldsymbol{\sigma}_c'^n}{\bar{\rho}_{s,FC}} - \frac{\nabla^{FC} P_{eq}}{\rho_s} + \mathbf{b} \right) \tag{32}$$

The equation (32) is discretized in three dimension(noted that $\nabla^{FC} \cdot \sigma_{ij} = 0$ with $i \neq j$), for example the discretized equation in the x direction is

$$U_{sx}^* = \frac{(\bar{\rho}U)_{sx,R}^n + (\bar{\rho}U)_{sx,L}^n}{\bar{\rho}_{sx,L}^n + \bar{\rho}_{sx,R}^n} + \Delta t \left(\frac{2(\sigma_{xx,R} - \sigma_{xx,L})}{(\bar{\rho}_{sx,L}^n + \bar{\rho}_{sx,R}^n)\Delta x} - \frac{P_{eqx,R} - P_{eqx,L}}{\rho_s \Delta x} + b_x \right) \quad (33)$$

Computing the modified faced-centered velocity \mathbf{U}_{FC}^L considering the momentum exchange

$$\begin{aligned} \mathbf{U}_{f,FC}^L &= \mathbf{U}_{f,FC}^* + \Delta \mathbf{U}_{f,FC} \\ \mathbf{U}_{s,FC}^L &= \mathbf{U}_{s,FC}^* + \Delta \mathbf{U}_{s,FC} \end{aligned} \quad (34)$$

By solving the linear equation below to obtain the increment of velocity

$$\begin{vmatrix} (1 + \beta_{12,FC}) & -\beta_{12,FC} \\ -\beta_{21,FC} & (1 + \beta_{21,FC}) \end{vmatrix} \begin{vmatrix} \Delta \mathbf{U}_{f,FC} \\ \Delta \mathbf{U}_{s,FC} \end{vmatrix} = \begin{vmatrix} \beta_{12,FC}(\mathbf{U}_{s,FC}^* - \mathbf{U}_{f,FC}^*) \\ \beta_{21,FC}(\mathbf{U}_{f,FC}^* - \mathbf{U}_{s,FC}^*) \end{vmatrix}$$

Compute advanced fluid pressure (implicit scheme)

We solve the generalized Poisson's equation below by employing a pre-conditioned conjugate gradient technique with a multi-grid pre-conditioner

$$\left(\kappa - \nabla^c \frac{\Delta t}{\bar{\rho}_{f,FC}} \cdot \nabla^{FC} \right) \Delta P_c^n = -\nabla^c \cdot \mathbf{U}_{f,FC}^L \quad (35)$$

The advanced fluid pressure at cell center is

$$P_c^{n+1} = P_{eq} + \Delta P_c^n \quad (36)$$

Finally, the faced-centered advanced fluid pressure is

$$P_{f,FC}^{n+1} = \left(\frac{P_{f,L}^{n+1}}{\bar{\rho}_{f,L}^n} + \frac{P_{f,R}^{n+1}}{\bar{\rho}_{f,R}^n} \right) / \left(\frac{1}{\bar{\rho}_{f,L}^n} + \frac{1}{\bar{\rho}_{f,R}^n} \right) = \left(\frac{P_{f,L}^{n+1} \bar{\rho}_{f,R}^n + P_{f,R}^{n+1} \bar{\rho}_{f,L}^n}{\bar{\rho}_{f,L}^n \bar{\rho}_{f,R}^n} \right) \quad (37)$$

Compute viscous shear stress term of the fluid phase

This part compute the viscous shear stress $\Delta(m\mathbf{U})_{fc,\tau}$ for a single viscous compressible Newtonian fluid and optionally shear stress induced by the turbulent model.

Compute nodal internal temperature of the solid phase

The nodal internal temperature rate is computed based on the heat conduction model

$$dT_{si}^L = \frac{(\Delta W_{si}^n + \nabla^i \cdot \mathbf{q}_{si}^n)}{m_{si}^n} \quad (38)$$

where $\Delta W_{si}^n = \boldsymbol{\sigma}' : \nabla \mathbf{U}_s$ is the mechanical work rate computed from the constitutive model. The nodal internal temperature is calculated by

$$T_{si}^L = T_{si}^n + dT_{si}^L \quad (39)$$

Compute and integrate acceleration of the solid phase

After interpolating from material points to the nodes, the nodal acceleration and velocity are calculate by

$$\mathbf{a}_{si}^{L-} = \frac{\mathbf{f}_{si}^{int,n} + \mathbf{f}_{si}^{ext,n}}{m_{si}^n} + \mathbf{g} \quad (40)$$

$$\mathbf{U}_{si}^{L-} = \mathbf{U}_{si}^n + \mathbf{a}_{si}^{L-} \Delta t \quad (41)$$

Compute Lagrangian value (mass, momentum and energy)

For the fluid phase, the linear momentum rate, the energy rate are

$$\Delta(m\mathbf{U})_{fc} = V n_c^n \nabla^c P_{fc}^{n+1} + \Delta(m\mathbf{U})_{fc,\tau} + V \bar{\rho}_{fc}^n g \quad (42)$$

$$\Delta(me)_{fc} = V n_c^n P_{fc}^{n+1} \nabla^c \cdot \mathbf{U}_{f,FC}^* + \nabla^c \cdot \mathbf{q}_{fc}^n \quad (43)$$

The Lagrangian value of the mass, linear momentum and energy of fluid phase without momentum exchange are

$$m_{fc}^L = V \bar{\rho}_{fc}^n \quad (44)$$

$$(m\mathbf{U})_{fc}^{L-} = V \bar{\rho}_{fc}^n \mathbf{U}_{fc}^n + \Delta(m\mathbf{U})_{fc} \quad (45)$$

$$(me)_{fc}^{L-} = V \bar{\rho}_{fc}^n T_{fc}^n c_v + \Delta(me)_{fc} \quad (46)$$

For the solid phase, the Lagrangian value of the linear momentum and energy of solid phase are

$$m_{sc}^L = m_{sc}^n \quad (47)$$

$$(m\mathbf{U})_{sc}^{L-} = \sum S_{ci} m_{si}^n \mathbf{U}_{si}^{L-} + V(1 - n_c^n) \nabla^c P_{fc}^{n+1} \quad (48)$$

$$(me)_{sc}^{L-} = \sum S_{ci} m_{si}^n T_{si}^L \quad (49)$$

To consider the momentum exchange, the Lagrangian velocity is modified as

$$\begin{aligned} \mathbf{U}_{fc}^L &= \mathbf{U}_{fc}^{L-} + \Delta \mathbf{U}_{fc} \\ \mathbf{U}_{sc}^L &= \mathbf{U}_{sc}^{L-} + \Delta \mathbf{U}_{sc} \end{aligned} \quad (50)$$

where the cell-centered intermediate velocity can be calculated by

$$\begin{aligned} \mathbf{U}_{fc}^{L-} &= \frac{(m\mathbf{U})_{fc}^{L-}}{m_{fc}^L} \\ \mathbf{U}_{sc}^{L-} &= \frac{(m\mathbf{U})_{sc}^{L-}}{m_{sc}^L} \end{aligned} \quad (51)$$

And the increment of the velocity can be computed by solving the linear equation below

$$\begin{vmatrix} (1 + \beta_{12,c}) & -\beta_{12,c} \\ -\beta_{21,c} & (1 + \beta_{21,c}) \end{vmatrix} \begin{vmatrix} \Delta \mathbf{U}_{fc} \\ \Delta \mathbf{U}_{sc} \end{vmatrix} = \begin{vmatrix} \beta_{12,c}(\mathbf{U}_{sc}^{L-} - \mathbf{U}_{fc}^{L-}) \\ \beta_{21,c}(\mathbf{U}_{fc}^{L-} - \mathbf{U}_{sc}^{L-}) \end{vmatrix}$$

Finally, we obtain the cell-centered solid acceleration and temperature rate as

$$d\mathbf{U}_{sc}^L = \frac{(m\mathbf{U})_{sc}^L - (m\mathbf{U})_{sc}^n}{m_{sc}^L \Delta t} \quad (52)$$

$$dT_{sc}^L = \frac{(me)_{sc}^L - (me)_{sc}^n}{m_{sc}^L c_v \Delta t} \quad (53)$$

Compute Lagrangian specific volume of the fluid phase

To compute the Lagrangian value of the specific volume of the fluid phase, we need to compute the Lagrangian temperature rate as below

$$T_{fc}^{n+1} = \frac{(me)_{fc}^L}{m_{fc}^L c_v} \quad (54)$$

$$\frac{D_f T_{fc}}{Dt} = \frac{T_{fc}^{n+1} - T_{fc}^n}{\Delta t} \quad (55)$$

As such, the Lagrangian specific volume rate is

$$\Delta(mv)_{fc} = V \nabla^c \cdot ((1 - n_c^n) \mathbf{U}_{sc}^L + n_c^n \mathbf{U}_{fc}^L) \quad (56)$$

Finally, the Lagrangian specific volume is

$$(mv)_{fc}^L = V \bar{\rho}_{f,c}^n v_{fc}^n + \Delta(mv)_{fc} \quad (57)$$

Compute advection term and advance in time

The time advanced mass, linear momentum, energy and specific volume are:

$$m_{fc}^{n+1} = m_{fc}^L - \Delta t \text{Advection}(\bar{\rho}_{fc}^L, \mathbf{U}_{f,FC}^L) \quad (58)$$

$$(m\mathbf{U})_{fc}^{n+1} = (m\mathbf{U})_{fc}^L - \Delta t \text{Advection}((\bar{\rho}\mathbf{U})_{fc}^L, \mathbf{U}_{f,FC}^L) \quad (59)$$

$$(me)_{fc}^{n+1} = (me)_{fc}^L - \Delta t \text{Advection}((\bar{\rho}c_v T)_{fc}^L, \mathbf{U}_{f,FC}^L) \quad (60)$$

$$(mv)_{fc}^{n+1} = (mv)_{fc}^L - \Delta t \text{Advection}((\bar{\rho}v)_{fc}^L, \mathbf{U}_{f,FC}^L) \quad (61)$$

Finally, the state variables of the fluid phase of the next time step are

$$\bar{\rho}_{fc}^{n+1} = \frac{m_{fc}^{n+1}}{V} \quad (62)$$

$$\mathbf{U}_{fc}^{n+1} = \frac{(m\mathbf{U})_{fc}^{n+1}}{m_{fc}^{n+1}} \quad (63)$$

$$T_{fc}^{n+1} = \frac{(me)_{fc}^{n+1}}{m_{fc}^{n+1}} \quad (64)$$

$$v_{fc}^{n+1} = \frac{(mv)_{fc}^{n+1}}{m_{fc}^{n+1}} \quad (65)$$

Interpolate from cell to node of the solid phase

First we interpolate the acceleration, velocity and temperature to the node

$$\mathbf{a}_{si}^n = \sum S_{ci} d\mathbf{U}_{sc}^L \quad (66)$$

$$\mathbf{U}_{si}^{n+1} = \sum S_{ci} d\mathbf{U}_{sc}^L \Delta t \quad (67)$$

$$dT_{si}^n = \sum S_{ci} dT_{sc}^L \quad (68)$$

Then the boundary condition and contact forces are applied to the nodal velocity and the acceleration is modified by

$$\mathbf{a}_{si}^n = \frac{\mathbf{v}_{si}^{n+1} - \mathbf{v}_{si}^n}{\Delta t} \quad (69)$$

Update the particle variables

The state variables of the solid phase $[\mathbf{U}_{sp}^{n+1}, \mathbf{x}_{sp}^{n+1}, \nabla \mathbf{U}_{sp}^{n+1}, T_{sp}^{n+1}, \mathbf{F}_{sp}^{n+1}, V_{sp}^{n+1}]$ (velocity, position, velocity gradient, temperature, deformation gradient, volume) are updated here

$$\mathbf{U}_{sp}^{n+1} = \mathbf{U}_{sp}^n + \sum S_{sp} \mathbf{a}_{si}^n \Delta t \quad (70)$$

$$\mathbf{x}_{sp}^{n+1} = \mathbf{x}_{sp}^n + \sum S_{sp} \mathbf{U}_{si}^{n+1} \Delta t \quad (71)$$

$$\nabla \mathbf{U}_{sp}^{n+1} = \sum \nabla S_{sp} \mathbf{U}_{si}^{n+1} \quad (72)$$

$$T_{sp}^{n+1} = T_{sp}^n + \sum S_{sp} dT_{si}^n \Delta t \quad (73)$$

$$\mathbf{F}_{sp}^{n+1} = (\mathbf{I} + \nabla \mathbf{U}_{sp}^{n+1} \Delta t) \mathbf{F}_{sp}^n \quad (74)$$

$$V_{sp}^{n+1} = \det(\mathbf{F}_{sp}^{n+1}) V_{sp}^o \quad (75)$$

Finally, the effective stress $(\boldsymbol{\sigma}')^{n+1}$ is updated from the constitutive model.

Numerical examples

All input files and the analytical calculations in this section are provided in the Github repository ¹ for the reproduction of the numerical results.

Fluid Flow through isothermal porous media

Fluid flow through porous media is important in many engineering disciplines, like predicting water flow in soil. Fluid flow velocity in one dimension can be calculated from the porous media's hydraulic conductivity K as:

$$U_f = K \frac{\Delta p_f}{L} \quad (76)$$

If the Carman-Kozeny formula is adopted $F = 10\phi_s/(1-\phi_s)^2$, the hydraulic conductivity will be expressed as $K = d^2(1-\phi_s)^3/180\mu\phi_s^2$. Then, the analytical formula of average velocity in one dimension through the porous media is:

$$U_f = \frac{1}{n} \frac{d^2(1-\phi_s)^3}{180\mu\phi_s^2} \frac{\Delta p_f}{L} \quad (77)$$

¹https://github.com/QuocAnh90/Uintah_NTNU

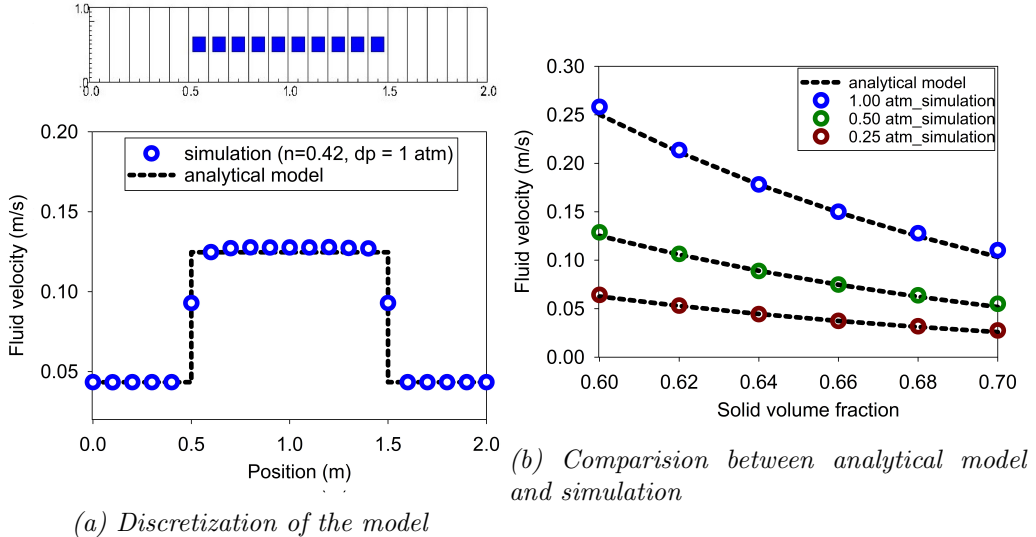


Figure 2: Numerical results of the fluid flow through isothermal porous media

Our numerical model is validated by modeling fluid flow through a 1m long porous media. This fluid has water properties (bulk modulus is 2GPa, density is 998 kg/m³ at 5 degrees Celsius and 10325 Pa (1atm) pressure, dynamic viscosity μ is 1mPa s). The porous media is modeled by elastic material with Young's modulus is 10 MPa, Poisson's ratio is 0.3, and density is 2650 kg/m³. The volume fraction of porous media ϕ_s is [0.6, 0.62, 0.66, 0.68, 0.7] and the average grain diameter d is 1mm. The model is discretized in 20 finite element and the porous media in 10 finite element with 1 material point per element. The pressure gradient is applied with three different value [0.25, 0.5, 1] atm. Figure 2 shows a good agreement of fluid flow prediction between the theory and the model.

Isothermal consolidation

A common benchmark fo a fully saturated porous meida is the simulation of one-dimensional consolidation. Using the Carman-Kozeny formula, the time-dependent pressure can be caluated as:

$$p_f = \sum_{m=1}^{\infty} \frac{2F_{ext}}{M} \sin\left(\frac{Mz}{H}\right) e^{-M^2 T_V} \text{ with } M = \frac{\pi}{2}(2m + 1) \quad (78)$$

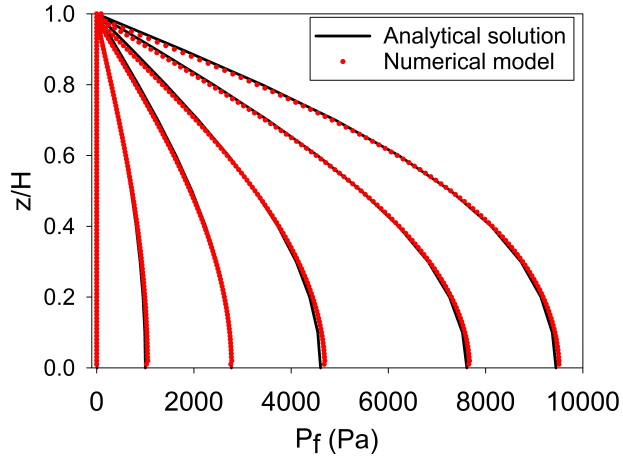


Figure 3: Comparison between analytical solution and numerical solution

where the consolidation rate $T_v = C_v t / H^2$, the consolidation coefficient $C_v = E_v n^3 d^2 / (180(1-n)^2 \mu)$ and the Oedometer modulus $E_v = E(1-v)/(1+v)/(1-2v)$. Our numerical model is validated by modeling the consolidation of a 1m column. This fluid has water properties (bulk modulus is 2GPa, density is 998 kg/m³ at 5 degrees Celsius and 10325 Pa (1atm) pressure, dynamic viscosity μ is 1mPa s). The porous media is modeled by elastic material with Young's modulus is 10 MPa, Poisson's ratio is 0.3, and density is 2650 kg/m³. The volume fraction of porous media ϕ_s is 0.7 which is equivalent to the porosity of 0.3 and the average grain diameter d is 1mm. The model is discretized in 100 finite element with 1 material point per element. The external pressure applies to the top of the column is 10 kPa. Figure 3 shows a good agreement of fluid flow prediction between the theory and the model.

Thermal induced cavity flow

Another benchmark is the thermal induced cavity flow in porous media. Temperature and velocity distributions are calculated for a square non-deformable saturated porous media. The top and bottom walls are insulated, and the left and right walls are at fixed temperatures differing by 1 C. The fluid motion at steady state are cavity flow due to the temperature induced density variation.

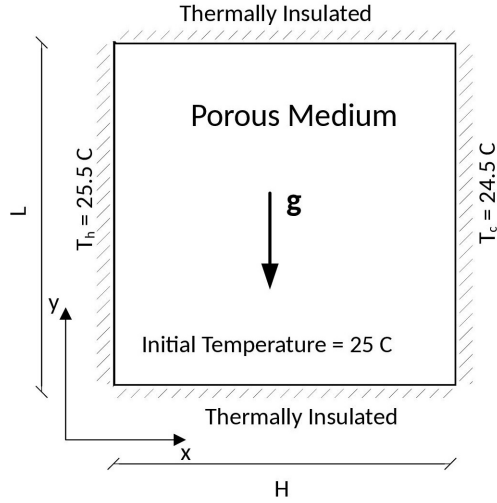


Figure 4: Model schematic

The numerical is validated by comparing with the numerical solution of the finite element method. The fluid has water properties (bulk modulus is 2GPa, density is 998 kg/m³ at 5 degrees Celsius and 10325 Pa (1atm) pressure, dynamic viscosity μ is 1 mPa s). The porous media is modeled by non deformable material, and density is 2500 kg/m³. The specific heat capacity of the water and porous skeleton are 4181 J/kg.K and 835 J/kg.K respectively. The thermal conductivity of the water and porous skeleton are 0.598 W/m.K and 0.4 W/m.K. The volume fraction of porous media ϕ_s is 0.6 which is equivalent to the porosity of 0.4 and the average grain diameter d is 1mm. The model is discretized in 20 x 20 finite element with 4 material point per element. Figure 5 shows a good agreement of numerical results of the model compared with the numerical solution of the finite element method.

Underwater debris flow

The numerical example is validated by Rzadkiewicz et al.'s experiment on submarine debris flow [17]. During the experiment, sand in a triangular box is released and then slides along a rigid bed inclined 45 degrees under water, see figure 6

In the numerical model, the material properties are selected based on the experiment by Rzadkiewicz et al [17]. Sand has a saturated density of 1985

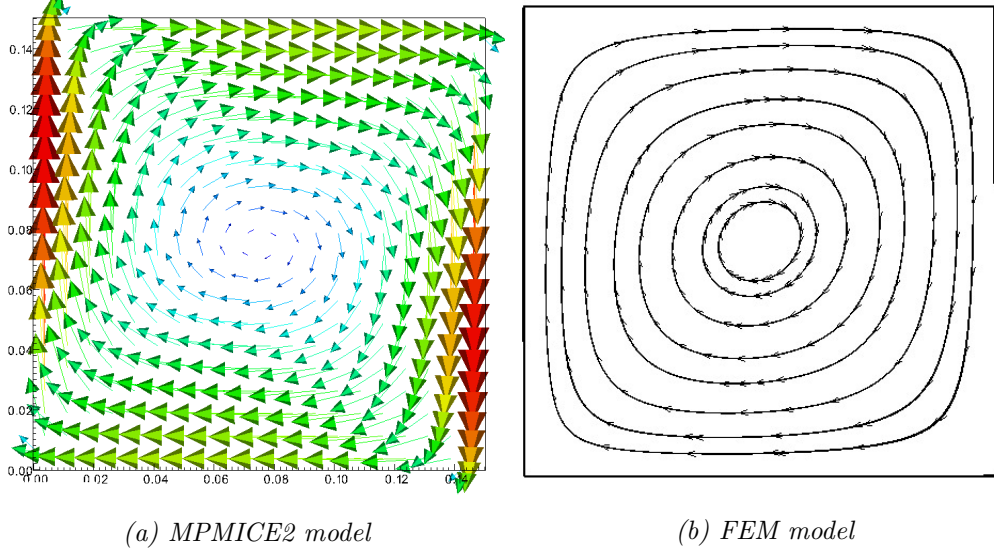


Figure 5: Comparision between MPMICE2 model and FEM model

kg/m^3 and yield stress of 200 Pa. Young's modulus has little effect on debris flow run-out because of the extreme large deformation of the debris. Therefore, we select 50 MPa Young's modulus with 0.25 Poisson's ratio. The rigid bed is much stiffer with bulk modulus and shear modulus of $117e^7$ Pa and $43.8e^7$ Pa. Under gravity, the density of the water at the surface is 999.8 kg/m^3 at the pressure of 1 atm. At the top boundary, the air has a density of 1.17 kg/m^3 at the atmospheric pressure of 1 atm. At 5 Celcius degrees, air and water have viscosities of $18.45e^{-3}$ mPa s and 1 mPa s respectively. The numerical parameters used in this example are presented in Table 1. On all boundary faces, the Dirichlet boundary condition is imposed for velocity ($u = 0 \text{ m/s}$) and temperature ($T = 5 \text{ Celcius degrees}$), while the Neuman boundary condition is imposed for pressure ($dp/dx = 0 \text{ kPa}$) and density ($d/dx = 0 \text{ kg/m}^3$). For the background mesh, there are $700 \times 400 = 280.000$ cells. In each cell of the debris flow and rigid bed, there are 2×2 material points.

Figure 7a and 7b show snapshots of the debris flow sliding in the plane at 0.4 s and 0.8 s. Our simulations match the computed results from Rzadkiewicz et al. [17]. The model also captures typical hydroplaning mechanism of the underwater debris flow (hydroplaning means the debris flow is lifted up and no longer in contact with the bottom layer). The elevation of the free

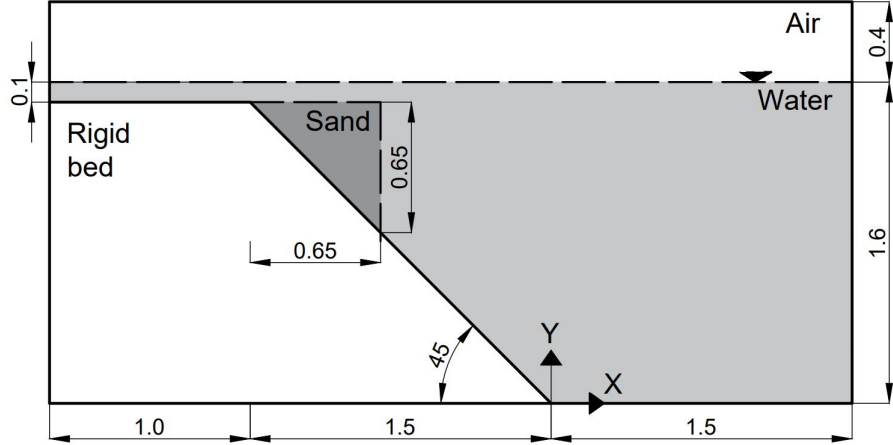


Figure 6: Model schematic

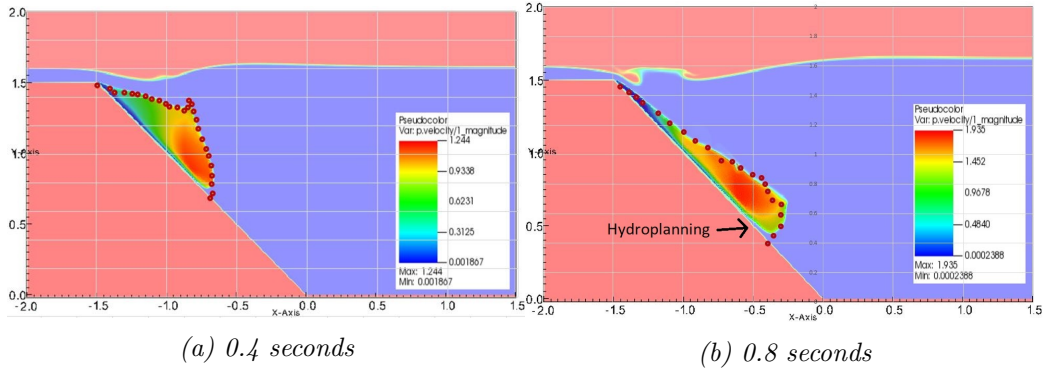


Figure 7: Simulation of underwater debris flow

surface at 0.4s and 0.8s is compared between our proposed method and other methods in Figure 8. Once again, our computed results were consistent with both the experiment and others computational results. Unlike other computational models based on total stress analysis, the proposed model based on the effective stress analysis which allows to analyze the water pressure and temperature in the debris flow.

We also explore the difference between underwater debris flow and saturated debris flow in terms of interacting with obstacle. Figure x shows the snapshot of the simulations of underwater and saturated debris flow. The saturated debris flow behaves like frictional flow as grain have contact forces with each other. On the other hand, the underwater debris flow behave like turbulent

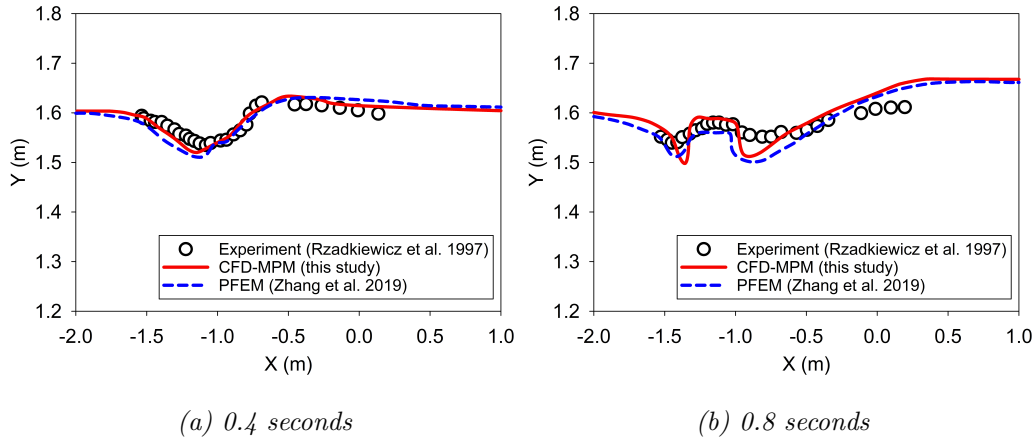


Figure 8: Simulation of underwater debris flow

flow as grains are separated from each other and exhibit no contact forces between grains.

Earthquake-induced submarine landslides

0-10-26-final

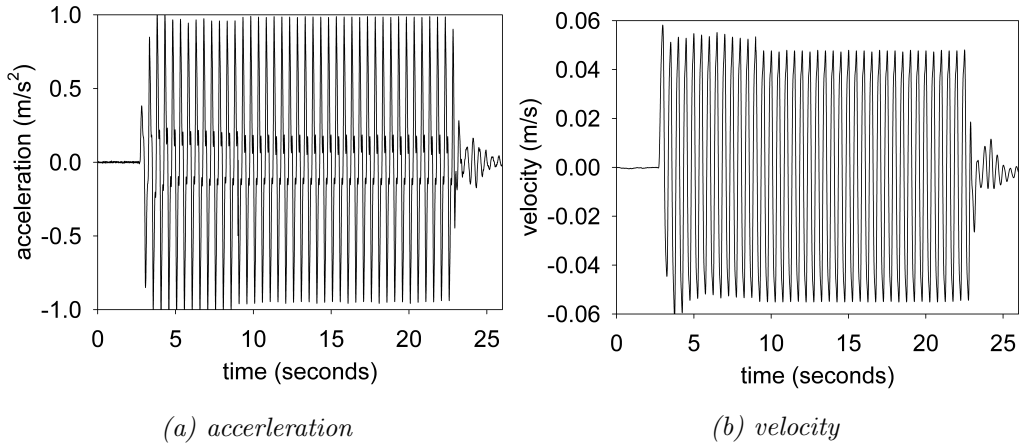


Figure 9: Ground acceleration profile, frequency of 2Hz and magnitude of 1g

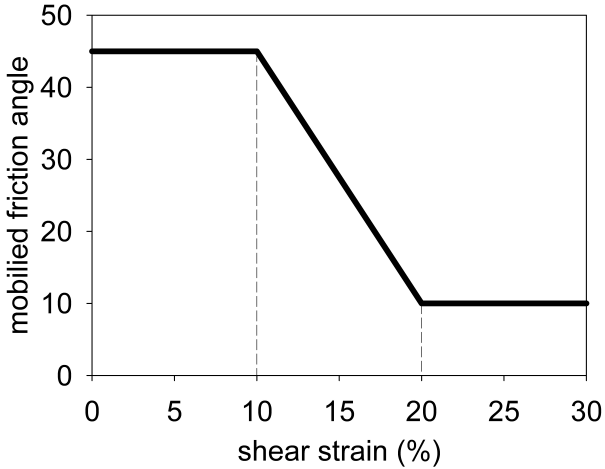


Figure 10: Mobilized friction angle in Mohr Coulomb model

Conclusions

Acknowledgements

This project has received funding from the European Union’s Horizon 2020 research and innovation program under the Marie Skłodowska-Curie Actions (MSCA) Individual Fellowship (Project SUBSLIDE “Submarine landslides and their impacts on offshore infrastructures”) grant agreement 101022007. The authors would also like to acknowledge the support from the Research Council of Norway through its Centers of Excellence funding scheme, project number 262644 Porelab. The computations were performed on High Performance Computing resources provided by UNINETT Sigma2 - the National Infrastructure for High Performance Computing and Data Storage in Norway.

Appendix

Before deriving the governing equation, we give some definition (following [18]) as below:

$$-\frac{1}{V} \left[\frac{\partial V}{\partial p} \right] \equiv \kappa_f \quad \text{isothermal compressibility of fluid} \quad (.1)$$

$$\frac{1}{V} \left[\frac{\partial V}{\partial T} \right] \equiv \alpha_f \quad \text{constant pressure thermal expansivity of fluid} \quad (.2)$$

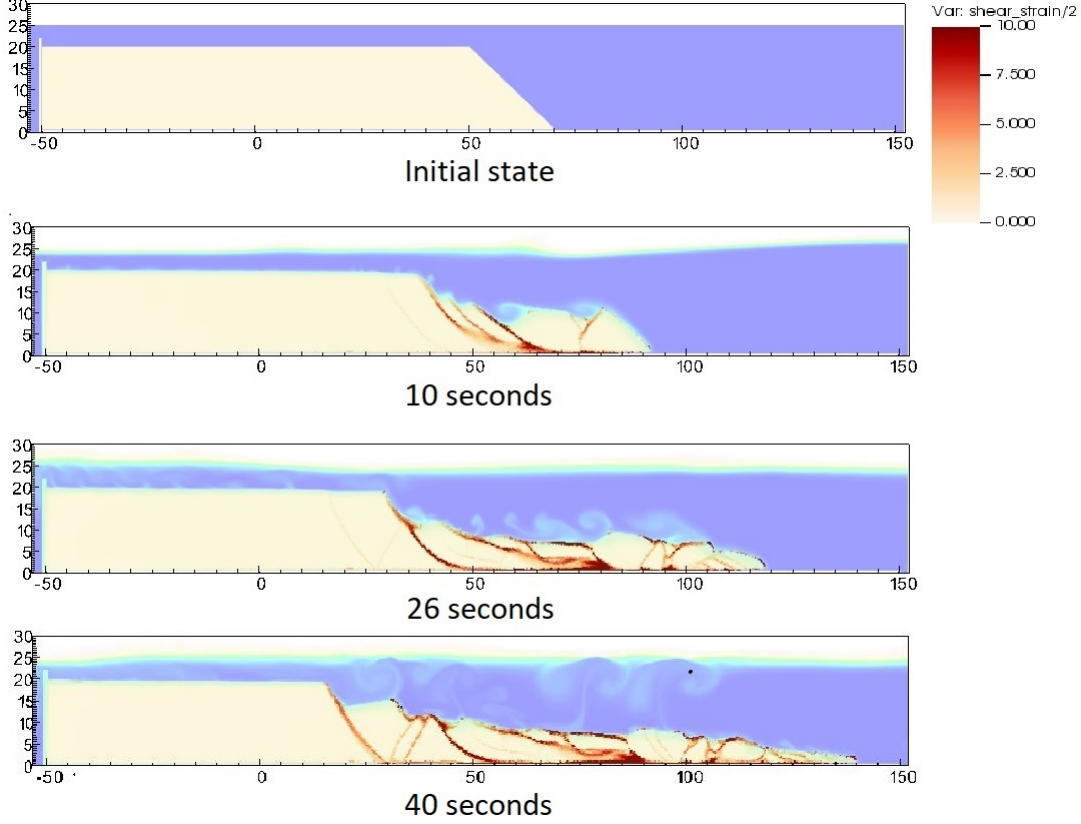


Figure 11: Shear strain during the earthquake-induced submarine landslides

Then, the rate of volume with incompressible solid grains are calculated as below:

$$\begin{aligned} \frac{1}{V} \frac{D_f V}{Dt} &= \frac{1}{V} \left(\left[\frac{\partial V}{\partial p} \right] \frac{D_f p}{Dt} + \left[\frac{\partial V}{\partial T} \right] \frac{D_f T}{Dt} \right) = \frac{1}{V} \left(-\kappa \frac{D_f p}{Dt} + \alpha \frac{D_f T}{Dt} \right) \quad (.3) \\ &= -(-\nabla \cdot \mathbf{U}_f + \alpha_f \frac{D_f T_f}{Dt}) + \alpha_f \frac{D_f T_f}{Dt} = \nabla \cdot \mathbf{U}_f \end{aligned}$$

$$\frac{1}{V} \frac{D_s V}{Dt} = \nabla \cdot \mathbf{U}_s \quad (.4)$$

It is also convenient to define the Lagrangian derivative for a state variable f as:

$$\frac{D_f f}{Dt} = \frac{\partial f}{\partial t} + \mathbf{U}_f \cdot \nabla f \quad \frac{D_s f}{Dt} = \frac{\partial f}{\partial t} + \mathbf{U}_s \cdot \nabla f \quad (.5)$$

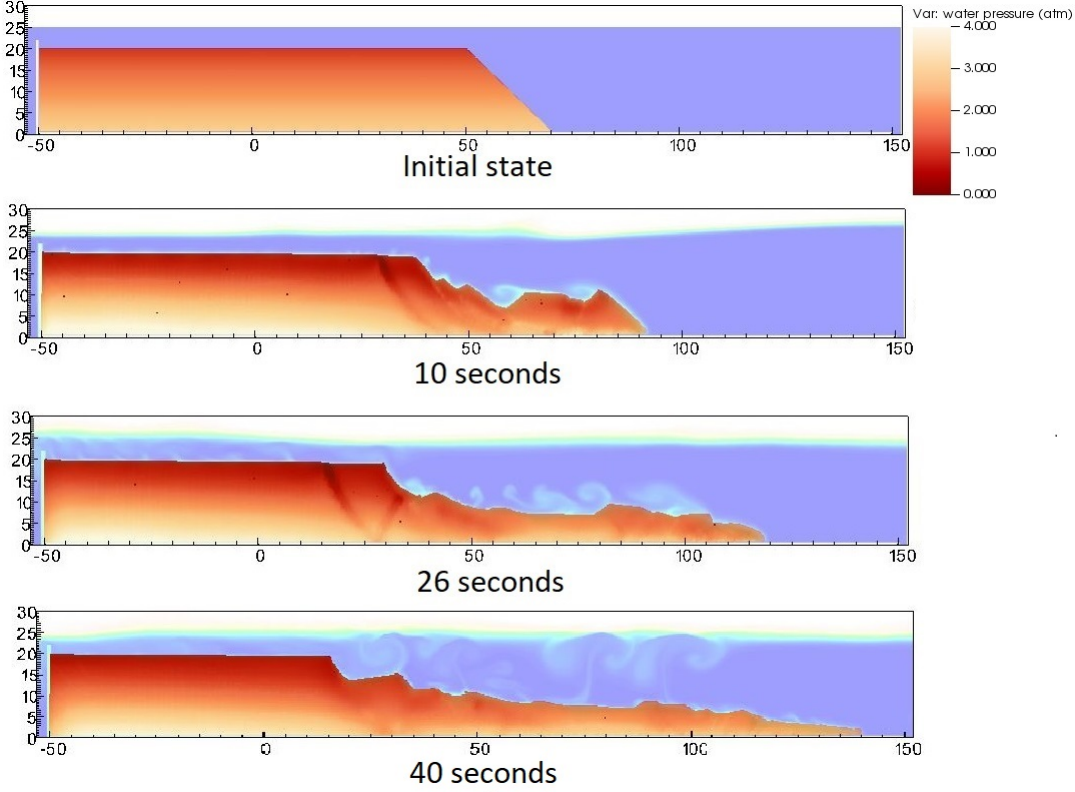


Figure 12: pore water pressure during the earthquake-induced submarine landslides

Evolution of porosity

Solving the solid mass balance equation (4) with the definition of solid mass in equation (2), it leads to the rate of porosity as below:

$$\frac{D_s m_s}{Dt} = \frac{D_s((1-n)\rho_s V)}{Dt} = \rho_s V \frac{D_s(1-n)}{Dt} + (1-n)V \frac{D_s \rho_s}{Dt} + (1-n)\rho_s \frac{D_s V}{Dt} = 0 \quad (.6)$$

The soil grains are assumed to be incompressible, therefore, term 2 in the right hand side is zero.

$$V \frac{D_s(1-n)}{Dt} + (1-n) \frac{D_s V}{Dt} = 0 \quad (.7)$$

Dividing all terms with V with the equation (.3), it leads to:

$$\frac{D_s n}{Dt} = \frac{\partial n}{\partial t} + \mathbf{U}_s \cdot \nabla n = (1-n) \nabla \cdot \mathbf{U}_s \quad (.8)$$

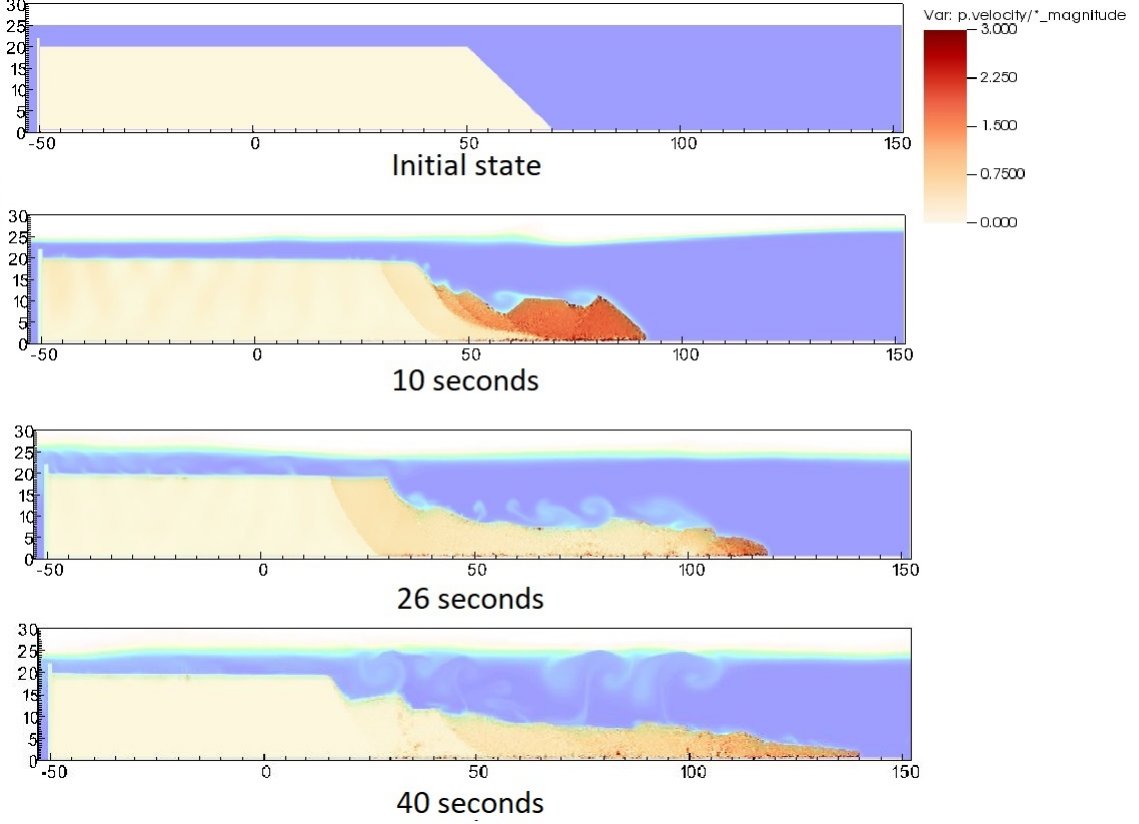


Figure 13: Velocity during the earthquake-induced submarine landslides

Finally, we get:

$$\frac{\partial n}{\partial t} = (1 - n)\nabla \cdot \mathbf{U}_s - \mathbf{U}_s \cdot \nabla n \quad (.9)$$

Evolution of specific volume

Solving the fluid mass balance equation (4) with the definition of fluid mass in equation (2), it leads to:

$$\frac{D_f m_f}{Dt} = \frac{D_f(n\rho_f V)}{Dt} = \rho_f V \frac{D_f n}{Dt} + nV \frac{D_f \rho_f}{Dt} + n\rho_f \frac{D_f V}{Dt} = 0 \quad (.10)$$

Dividing all terms with V and converting the fluid density ρ_f to the specific volume v_f , it becomes:

$$\frac{D_f n}{Dt} - \bar{\rho}_f \frac{D_f v_f}{Dt} + \frac{n}{V} \frac{D_f V}{Dt} = 0 \quad (.11)$$

The Lagrangian porosity can be written as:

$$\frac{D_f n}{Dt} = \frac{\partial n}{\partial t} + \mathbf{U}_f \cdot \nabla n \quad (.12)$$

Combining equations (.3), (.9), (.11), (.12) we get:

$$\bar{\rho}_f \frac{D_f v_f}{Dt} = \nabla \cdot ((1-n)\mathbf{U}_s + n\mathbf{U}_f) \quad (.13)$$

Momentum conservation

The linear momentum balance equation for the fluid phase based on mixture theory is:

$$\frac{1}{V} \frac{D_f(m_f \mathbf{U}_f)}{Dt} = \nabla \cdot (-np_f \mathbf{I}) + \nabla \cdot \boldsymbol{\tau}_f + \bar{\rho}_f \mathbf{b} + \mathbf{f}_d + \mathbf{f}_b \quad (.14)$$

On the right hand side, the first term is the divergence of partial fluid phase stress, the second term is the body force, the third term is the drag force (momentum exchange) and the fourth term is the buoyant force described in [19] for the immiscible mixtures. The buoyant force is in the form:

$$\mathbf{f}_b = \boldsymbol{\sigma}_f \nabla(n) \quad (.15)$$

As a result, the linear momentum balance equation for fluid phase becomes:

$$\frac{1}{V} \frac{D_f(m_f \mathbf{U}_f)}{Dt} = -n \nabla p_f + \nabla \cdot \boldsymbol{\tau}_f + \bar{\rho}_f \mathbf{b} + \mathbf{f}_d \quad (.16)$$

The Reynolds stress component can be included in the term $\boldsymbol{\tau}_f$ to consider the turbulent effects if needed. To derive the linear momentum balance equation for the solid phase, we begin with the linear momentum balance equation for the mixture as:

$$\frac{1}{V} \frac{D_f(m_f \mathbf{U}_f)}{Dt} + \frac{1}{V} \frac{D_s(m_s \mathbf{U}_s)}{Dt} = \nabla \cdot (\boldsymbol{\sigma}) + \bar{\rho}_f \mathbf{b} + \bar{\rho}_s \mathbf{b} \quad (.17)$$

Combining Terzaghi's equation (3) and subtracting both sides with equation (.16), we obtain the linear momentum balance equation for the solid phase as:

$$\nabla \cdot (\boldsymbol{\sigma}') - (1-n) \nabla p_f + \bar{\rho}_s \mathbf{b} - \mathbf{f}_d \quad (.18)$$

Energy conservation

We adopt the general form of the total energy balance equation for the porous media from [20], the total energy balance equation for the fluid phase is:

$$\frac{1}{V} \frac{D_f(m_f(e_f + 0.5\mathbf{U}_f^2))}{Dt} = \nabla \cdot (-np_f \mathbf{I}) \cdot \mathbf{U}_f + \nabla \cdot \mathbf{q}_f + (\bar{\rho}_f \mathbf{b}) \cdot \mathbf{U}_f + \mathbf{f}_d \cdot \mathbf{U}_f + q_{sf} \quad (.19)$$

Applying the product rule $D(m\mathbf{U}^2) = D(m\mathbf{U} \cdot \mathbf{U}) = 2\mathbf{U} \cdot D(m\mathbf{U})$, the left hand side of equation (.19) becomes:

$$\frac{1}{V} \frac{D_f(m_f(e_f + 0.5\mathbf{U}_f^2))}{Dt} = \frac{1}{V} \frac{D_f(m_f e_f)}{Dt} + \frac{1}{V} \frac{D_f(m_f \mathbf{U}_f)}{Dt} \cdot \mathbf{U}_f \quad (.20)$$

Combining equations (.16), (.19), (.20), we obtain the final form of the internal energy balance equation for the fluid phase as:

$$\frac{1}{V} \frac{D_f(m_f e_f)}{Dt} = -\bar{\rho}_f p \frac{D_f v_f}{Dt} + \nabla \cdot \mathbf{q}_f + q_{sf} \quad (.21)$$

On the right hand side, the terms include the average pressure-volume work, the average viscous dissipation, the thermal transport and the energy exchange between solid and fluid respectively. The heat flux is $\mathbf{q}_f = \bar{\rho}_f \alpha_f \nabla T_f$. To derive the internal energy balance equation for the solid phase, we begin with the total energy balance equation for the mixture based on [20] as:

$$\begin{aligned} \frac{1}{V} \frac{D_f(m_f(e_f + 0.5\mathbf{U}_f^2))}{Dt} + \frac{1}{V} \frac{D_s(m_s(e_s + 0.5\mathbf{U}_s^2))}{Dt} &= \nabla \cdot (-np_f \mathbf{I}) \cdot \mathbf{U}_f \\ &+ \nabla \cdot (\boldsymbol{\sigma}' - (1-n)p_f \mathbf{I}) \cdot \mathbf{U}_s + (-np_f \mathbf{I}) : \nabla \mathbf{U}_f + (\boldsymbol{\sigma}' - (1-n)p_f \mathbf{I}) : \nabla \mathbf{U}_s \\ &+ (\bar{\rho}_f \mathbf{b}) \cdot \mathbf{U}_f + (\bar{\rho}_s \mathbf{b}) \cdot \mathbf{U}_s + \nabla \cdot \mathbf{q}_f + \nabla \cdot \mathbf{q}_s + \mathbf{f}_d \cdot (\mathbf{U}_f - \mathbf{U}_s) \end{aligned} \quad (.22)$$

Subtracting equation (.22) to equations (.19) and (.18), we obtained the internal energy balance equation for solid phase as:

$$\frac{1}{V} \frac{D_s(m_s e_s)}{Dt} = \boldsymbol{\sigma}' : \nabla \mathbf{U}_s + \nabla \cdot \mathbf{q}_s - q_{sf} \quad (.23)$$

On the right hand side, the terms include the mechanical work, thermal transport and energy exchange between solid and fluid respectively. The heat flux is $\mathbf{q}_s = \bar{\rho}_s \alpha_s \nabla T_s$

Advanced Fluid Pressure

The discretization of the pressure equation begins with the Lagrangian face-centered velocity and the equation for the pressure

$$\bar{\rho}_{f,FC} \frac{\mathbf{U}_{f,FC}^{n+1} - \mathbf{U}_{f,FC}^n}{dt} = n \nabla^{FC} P_{fc}^{n+1} + \bar{\rho}_{f,FC} \mathbf{b} \quad (.24)$$

$$\kappa \frac{dP}{dt} = \nabla^c \cdot \mathbf{U}_{f,FC}^{n+1} \quad (.25)$$

The divergence of the equation (.24) with $\nabla \cdot \mathbf{b} = 0$ is

$$\nabla^c \cdot \mathbf{U}_{f,FC}^{n+1} - \nabla^c \cdot \mathbf{U}_{f,FC}^n = \nabla^c \frac{\Delta t}{\rho_{f,FC}^n} \cdot \nabla^{FC} (P_{fc}^n + \Delta P_{fc}^n) \quad (.26)$$

To solve this equation, we define the face-centered intermediate velocity $\mathbf{U}_{f,FC}^*$ as:

$$\bar{\rho}_{f,FC} \frac{\mathbf{U}_{f,FC}^* - \mathbf{U}_{f,FC}^n}{\Delta t} = n \nabla^{FC} P_{fc}^n + \bar{\rho}_{f,FC} \mathbf{b} \quad (.27)$$

The divergence of the equation (.27) is

$$\nabla^c \cdot \mathbf{U}_{f,FC}^* - \nabla^c \cdot \mathbf{U}_{f,FC}^n = \nabla^c \frac{\Delta t}{\rho_{f,FC}^n} \cdot \nabla^{FC} P_{fc}^n \quad (.28)$$

Combining equations (.25, .26, .28), it leads to

$$\left(\kappa - \nabla^c \frac{\Delta t}{\rho_{f,FC}^n} \cdot \nabla^{FC} \right) \Delta P_{fc}^n = -\nabla^c \cdot \mathbf{U}_{f,FC}^* \quad (.29)$$

When the fluid is incompressible, κ approaches to zero and the equation (.29) becomes the Poisson's equation for the incompressible fluid flow.

Momentum exchange with an implicit solve

Considering the fluid momentum balance equation as

$$(m\mathbf{U})_{f,FC}^{n+1} = (m\mathbf{U})_{f,FC}^n - \Delta t (Vn \nabla^{FC} P_{fc}^n + m_f \mathbf{b}) + VK \Delta t (\mathbf{U}_{s,FC}^{n+1} - \mathbf{U}_{f,FC}^{n+1}) \quad (.30)$$

Assuming $m_{f,FC}^{n+1} = m_{f,FC}^n$ we get

$$\mathbf{U}_{f,FC}^{n+1} = \mathbf{U}_{f,FC}^n - \Delta t \left(\frac{\nabla^{FC} P_{fc}^n}{\rho_{f,FC}^n} + \mathbf{b} \right) + \frac{\Delta t K}{\bar{\rho}_{f,FC}^n} (\mathbf{U}_{s,FC}^{n+1} - \mathbf{U}_{f,FC}^{n+1}) \quad (.31)$$

As defined in the section 'Advanced Fluid Pressure', the face-centered intermediate fluid velocity $\mathbf{U}_{f,FC}^* = \Delta t(\nabla^{FC} P_{fc}^n / \rho_{f,FC}^n + \mathbf{b})$ leading to

$$\mathbf{U}_{f,FC}^{n+1} = \mathbf{U}_{f,FC}^* + \frac{\Delta t K}{\bar{\rho}_{f,FC}^n} (\mathbf{U}_{s,FC}^{n+1} - \mathbf{U}_{f,FC}^{n+1}) \quad (.32)$$

Considering the solid momentum balance equation as

$$(m\mathbf{U})_{s,FC}^{n+1} = (m\mathbf{U})_{s,FC}^n - \Delta t(V\nabla^{FC} \cdot \boldsymbol{\sigma}'^n - V(1-n)\nabla^{FC} P_{fc}^n + m_s \mathbf{b}) - VK\Delta t(\mathbf{U}_{s,FC}^{n+1} - \mathbf{U}_{f,FC}^{n+1}) \quad (.33)$$

We define the face-centered intermediate solid velocity as $\mathbf{U}_{s,FC}^* = \Delta t(\nabla^{FC} \cdot \boldsymbol{\sigma}_c'^n / \bar{\rho}_{s,FC} - \nabla^{FC} P_{fc}^n / \rho_s + \mathbf{b})$ leading to

$$\mathbf{U}_{s,FC}^{n+1} = \mathbf{U}_{s,FC}^* - \frac{\Delta t K}{\bar{\rho}_{s,FC}^n} (\mathbf{U}_{s,FC}^{n+1} - \mathbf{U}_{f,FC}^{n+1}) \quad (.34)$$

Combining equation (.32) and (.34) we get

$$\begin{aligned} \mathbf{U}_{f,FC}^* + \Delta\mathbf{U}_{f,FC} &= \mathbf{U}_{f,FC}^* + \frac{\Delta t K}{\bar{\rho}_{f,FC}^n} (\mathbf{U}_{s,FC}^* + \Delta\mathbf{U}_{s,FC} - \mathbf{U}_{f,FC}^* - \Delta\mathbf{U}_{f,FC}) \\ \mathbf{U}_{s,FC}^* + \Delta\mathbf{U}_{s,FC} &= \mathbf{U}_{s,FC}^* - \frac{\Delta t K}{\bar{\rho}_{s,FC}^n} (\mathbf{U}_{s,FC}^* + \Delta\mathbf{U}_{s,FC} - \mathbf{U}_{f,FC}^* - \Delta\mathbf{U}_{f,FC}) \end{aligned} \quad (.35)$$

Rearranging the equation (.35), it leads to the linear system of equations

$$\begin{vmatrix} (1 + \beta_{12,FC}) & -\beta_{12,FC} \\ -\beta_{21,FC} & (1 + \beta_{21,FC}) \end{vmatrix} \begin{vmatrix} \Delta\mathbf{U}_{f,FC} \\ \Delta\mathbf{U}_{s,FC} \end{vmatrix} = \begin{vmatrix} \beta_{12,FC}(\mathbf{U}_{s,FC}^* - \mathbf{U}_{f,FC}^*) \\ \beta_{21,FC}(\mathbf{U}_{f,FC}^* - \mathbf{U}_{s,FC}^*) \end{vmatrix}$$

Solving this linear equations with $\beta_{12,FC} = (\Delta t K) / \bar{\rho}_{f,FC}^n$ and $\beta_{21,FC} = (\Delta t K) / \bar{\rho}_{s,FC}^n$. Similar derivation can be performed to computed the cell-center velocity increment leading to

$$\begin{vmatrix} (1 + \beta_{12c}) & -\beta_{12c} \\ -\beta_{21c} & (1 + \beta_{21c}) \end{vmatrix} \begin{vmatrix} \Delta\mathbf{U}_{fc} \\ \Delta\mathbf{U}_{sc} \end{vmatrix} = \begin{vmatrix} \beta_{12c}(\mathbf{U}_{sc}^* - \mathbf{U}_{fc}^*) \\ \beta_{21c}(\mathbf{U}_{fc}^* - \mathbf{U}_{sc}^*) \end{vmatrix}$$

with $\beta_{12c} = (\Delta t K) / \bar{\rho}_{fc}^n$ and $\beta_{21c} = (\Delta t K) / \bar{\rho}_{sc}^n$ and the cell-centered intermediate velocity can be calculated by

$$\begin{aligned} \mathbf{U}_{fc}^* &= \mathbf{U}_{fc}^n + \Delta t \left(-\frac{\nabla P_{fc}^{n+1}}{\rho_{fc}^n} + \frac{\nabla \cdot \boldsymbol{\tau}_{fc}^n}{\bar{\rho}_{fc}^n} + \mathbf{b} \right) \\ \mathbf{U}_{sc}^* &= \mathbf{U}_{sc}^n + \Delta t \left(\frac{\nabla \cdot \boldsymbol{\sigma}_c'^n}{\bar{\rho}_{sc}^n} - \frac{\nabla P_{fc}^{n+1}}{\rho_s} + \mathbf{b} \right) \end{aligned} \quad (.36)$$

References

- [1] D. Yuk, S. Yim, P.-F. Liu, Numerical modeling of submarine mass-movement generated waves using RANS model, *Computers and Geosciences* 32 (7) (2006) 927–935. doi:10.1016/j.cageo.2005.10.028.
URL <https://doi.org/10.1016/j.cageo.2005.10.028>
- [2] S. Glimsdal, J.-S. L'Heureux, C. B. Harbitz, F. Løvholt, The 29th january 2014 submarine landslide at statland, norway—landslide dynamics, tsunami generation, and run-up, *Landslides* 13 (6) (2016) 1435–1444. doi:10.1007/s10346-016-0758-7.
URL <https://doi.org/10.1007/s10346-016-0758-7>
- [3] S. Abadie, D. Morichon, S. Grilli, S. Glockner, Numerical simulation of waves generated by landslides using a multiple-fluid navier–stokes model, *Coastal Engineering* 57 (9) (2010) 779–794. doi:10.1016/j.coastaleng.2010.03.003.
URL <https://doi.org/10.1016/j.coastaleng.2010.03.003>
- [4] M. Rauter, S. Viroulet, S. S. Gylfadóttir, W. Fellin, F. Løvholt, Granular porous landslide tsunami modelling – the 2014 lake askja flank collapse, *Nature Communications* 13 (1) (Feb. 2022). doi:10.1038/s41467-022-28296-7.
URL <https://doi.org/10.1038/s41467-022-28296-7>
- [5] Q.-A. Tran, W. Sołowski, Generalized interpolation material point method modelling of large deformation problems including strain-rate effects – application to penetration and progressive failure problems, *Computers and Geotechnics* 106 (2019) 249–265. doi:10.1016/j.compgeo.2018.10.020.
URL <https://doi.org/10.1016/j.compgeo.2018.10.020>
- [6] T. Capone, A. Panizzo, J. J. Monaghan, SPH modelling of water waves generated by submarine landslides, *Journal of Hydraulic Research* 48 (sup1) (2010) 80–84. doi:10.1080/00221686.2010.9641248.
URL <https://doi.org/10.1080/00221686.2010.9641248>
- [7] X. Zhang, E. Oñate, S. A. G. Torres, J. Bleyer, K. Krabbenhoft, A unified lagrangian formulation for solid and fluid dynamics and its possibility for modelling submarine landslides and their consequences, Com-

- puter Methods in Applied Mechanics and Engineering 343 (2019) 314–338. doi:10.1016/j.cma.2018.07.043.
URL <https://doi.org/10.1016/j.cma.2018.07.043>
- [8] R. Dey, B. C. Hawlader, R. Phillips, K. Soga, Numerical modelling of submarine landslides with sensitive clay layers, *Géotechnique* 66 (6) (2016) 454–468. doi:10.1680/jgeot.15.p.111.
URL <https://doi.org/10.1680/jgeot.15.p.111>
- [9] S. Bandara, K. Soga, Coupling of soil deformation and pore fluid flow using material point method, *Computers and Geotechnics* 63 (2015) 199–214. doi:10.1016/j.compgeo.2014.09.009.
URL <https://doi.org/10.1016/j.compgeo.2014.09.009>
- [10] A. P. Tampubolon, T. Gast, G. Klár, C. Fu, J. Teran, C. Jiang, K. Museth, Multi-species simulation of porous sand and water mixtures, *ACM Transactions on Graphics* 36 (4) (2017) 1–11. doi:10.1145/3072959.3073651.
URL <https://doi.org/10.1145/3072959.3073651>
- [11] A. S. Baumgarten, K. Kamrin, A general constitutive model for dense, fine-particle suspensions validated in many geometries, *Proceedings of the National Academy of Sciences* 116 (42) (2019) 20828–20836. doi:10.1073/pnas.1908065116.
URL <https://doi.org/10.1073/pnas.1908065116>
- [12] Q.-A. Tran, W. Sołowski, Temporal and null-space filter for the material point method, *International Journal for Numerical Methods in Engineering* 120 (3) (2019) 328–360. doi:10.1002/nme.6138.
URL <https://doi.org/10.1002/nme.6138>
- [13] X. Zheng, F. Pisanò, P. J. Vardon, M. A. Hicks, An explicit stabilised material point method for coupled hydromechanical problems in two-phase porous media, *Computers and Geotechnics* 135 (2021) 104112. doi:10.1016/j.compgeo.2021.104112.
URL <https://doi.org/10.1016/j.compgeo.2021.104112>
- [14] Q. A. Tran, W. Sołowski, M. Berzins, J. Guilkey, A convected particle least square interpolation material point method, *International Journal for Numerical Methods in Engineering* 121 (6) (2019) 1068–1100.

doi:10.1002/nme.6257.

URL <https://doi.org/10.1002/nme.6257>

- [15] J.-S. Chen, M. Hillman, S.-W. Chi, Meshfree methods: Progress made after 20 years, *Journal of Engineering Mechanics* 143 (4) (Apr. 2017). doi:10.1061/(asce)em.1943-7889.0001176.
URL [https://doi.org/10.1061/\(asce\)em.1943-7889.0001176](https://doi.org/10.1061/(asce)em.1943-7889.0001176)
- [16] J. A. M. K. R. Beetstra, M. A. van der Hoef, Drag force of intermediate reynolds number flow past mono- and bidisperse arrays of spheres, *Fluid Mechanics and Transport Phenomena* 53 (2) (2007) 489 – 501. doi:<https://doi.org/10.1002/aic.11065>.
- [17] S. A. R. C. Mariotti;, P. Heinrich, Numerical simulation of submarine landslides and their hydraulic effects, *Journal of Waterway, Port, Coastal, and Ocean Engineering* 123 (4) (1997). doi:[https://doi.org/10.1061/\(ASCE\)0733-950X\(1997\)123:4\(149\)](https://doi.org/10.1061/(ASCE)0733-950X(1997)123:4(149)).
- [18] B. A. Kashiwa, A multifield model and method for fluid-structure interaction dynamics, Tech. Rep. LA-UR-01-1136, Los Alamos National Laboratory (2001).
- [19] D. Drumheller, On theories for reacting immiscible mixtures, *International Journal of Engineering Science* 38 (3) (2000) 347 – 382. doi:[https://doi.org/10.1016/S0020-7225\(99\)00047-6](https://doi.org/10.1016/S0020-7225(99)00047-6).
URL <http://www.sciencedirect.com/science/article/pii/S0020722599000476>
- [20] S. Hassanzadeh, Derivation of basic equations of mass transport in porous media, part1: Macroscopic balance laws, *Advances in Water Resources* 9 (1986) 196–206. doi:[https://doi.org/10.1016/0309-1708\(86\)90024-2](https://doi.org/10.1016/0309-1708(86)90024-2).